Ultrafast growth of wadsleyite in shock-produced melts and its implications for early solar system impact processes

Oliver Tschauner[a,b], Paul D. Asimow[b], Natalya Kostandova[b], Thomas J. Ahrens[b,c,1], Chi Ma[b], Stanislas Sinogeikin[d], Zhenxian Liu[e], Sirine Fakra[f], and Nobumichi Tamura[f]

[a]High Pressure Science and Engineering Center, Department of Physics, University of Nevada, Las Vegas, NV 89154; [b]Division of Geological and Planetary Sciences, and [c]Lindhurst Laboratory of Experimental Geophysics, Seismological Laboratory, California Institute of Technology, Pasadena, CA 91125; [d]High Pressure Collaborative Access Team, Advanced Photon Source, Argonne National Laboratory, Argonne, IL 60439; [e]Geophysical Laboratory, Carnegie Institution of Washington, Washington, DC 20015; and [f]Advanced Light Source, Lawrence Berkeley National Laboratory, Berkeley, CA 94720

We observed micrometer-sized grains of wadsleyite, a high-pressure phase of $(Mg,Fe)_2SiO_4$, in the recovery products of a shock experiment. We infer these grains crystallized from shock-generated melt over a time interval of <1 μs, the maximum time over which our experiment reached and sustained pressure sufficient to stabilize this phase. This rapid crystal growth rate (≈ 1 m/s) suggests that, contrary to the conclusions of previous studies of the occurrence of high-pressure phases in shock-melt veins in strongly shocked meteorites, the growth of high-pressure phases from the melt during shock events is not diffusion-controlled. Another process, such as microturbulent transport, must be active in the crystal growth process. This result implies that the times necessary to crystallize the high-pressure phases in shocked meteorites may correspond to shock pressure durations achieved on impacts between objects 1–5 m in diameter and not, as previously inferred, ≈ 1–5 km in diameter. These results may also provide another pathway for syntheses, via shock recovery, of some high-value, high-pressure phases.

meteorite | recovery | high-pressure phases | planetesimal growth | shock experiments

A number of high-pressure silicate phases that stably occur only in the Earth's deep interior have documented natural occurrences, most commonly within shock-induced melt veins in L- and H-chondrites and Martian meteorites, notably the highly shocked (S6) Peace River, Tenham, Sixiangkou, and Yamato 791384 meteorites. Such phases include lingunite (the high-pressure polymorph of $NaAlSi_3O_8$ in the hollandite structure) (1, 2); stishovite and poststishovite silica phases (3–5); wadsleyite (6) and ringwoodite (7), the high-pressure polymorphs of $(Mg,Fe)_2SiO_4$ in a spinelloid (wadsleyite) and the spinel structure (ringwoodite), respectively; and $(Mg,Fe)SiO_3$ in the garnet [majorite (8, 9)], ilmenite [akimotoite (10)], and arguably the perovskite structure (11, 12). Pressures of formation have been estimated from static synthesis experiments of such phases and range up to 26 GPa (12–16). However, only stishovite has been recovered from shock experiments with very rapid quench and only in small amounts (17–19). None of the other dense silicate phases (wadsleyite, ringwoodite, majorite, lingunite, akimotoite, or perovskite) has been recovered from shock experiments conducted up to megabar pressures (20). These negative laboratory results in combination with observations of texture and paragenesis of high-pressure silicate polymorphs in meteorites have been used to infer the durations of shock-induced high-pressure, high-temperature conditions to be on the order of seconds to minutes (15, 21–24). In particular, this conclusion has been based on the grain size of these minerals (15), the width of lamellae within partly converted phases (21, 22), and diffusion profiles of trace or major elements across phase boundaries (23, 24) between high-pressure minerals occurring within shock-induced melt veins of meteorites. Seconds- to minutes-long high-pressure durations are not achievable in laboratory-scale shock experiments, which is generally considered one of the principal reasons for the failure to recover these phases in experiments (12, 20, 25). If long shock durations are in fact required to form and preserve the meteoritic occurrences, it implies that the shocks recorded are the result of impacts between large objects [5 km and larger (22–24, 26)] and imposes a significant constraint on the relationship between planetesimal size and relative impact velocity during the impact accretion phase of solar nebula evolution.

We demonstrate here that high-pressure silicate polymorphs, in particular wadsleyite, can be synthesized and recovered in shock experiments on a time scale of <1 μs. Because wadsleyite occurs in a number of meteorites that are believed to be remains of the planetesimals that accreted to form planets this result has significant implications on the time scales of planetesimal growth rates in the solar nebula.

Experiments

Our shock recovery experiment was conducted on a doubly polished disk of 500-μm thickness of porous MgO (bulk density, 2.30 g/cm^3) placed in contact with a similarly shaped disk of fused quartz. The 2 disks were then encased in a stainless-steel recovery chamber for shock loading. A tantalum flyer plate launched at 1.53 km/s imparted a shock into the sample chamber. From impedance matching, we calculated a final shock pressure of 26 GPa in the steel container and assumed that multiple reverberations of the shock within the sample cavity also achieve this pressure. Calculations using the thickness of the Ta flyer plate and the shock and rarefaction velocities in stainless steel and Ta yielded a total duration of ≈ 700 ns. The time required for 2 reverberations to traverse the sample chamber implies that the sample only achieved shock pressures >16 GPa for ≈ 500 ns. The peak temperature of the initially porous MgO has been estimated at 2,000–3,000 K (27). The shocked material was retrieved by cutting the container open with a water-cooled diamond saw.

We examined the sample by electron microprobe (EMP) mapping, spatially resolving micro X-ray diffractometry at the synchrotron beamline 16-Insertion Device B (High Pressure Collaborative Access Team), Advanced Photon Source, and the microdiffraction beamline 7.3.3, Advanced Light Source; IR

GEOPHYSICS
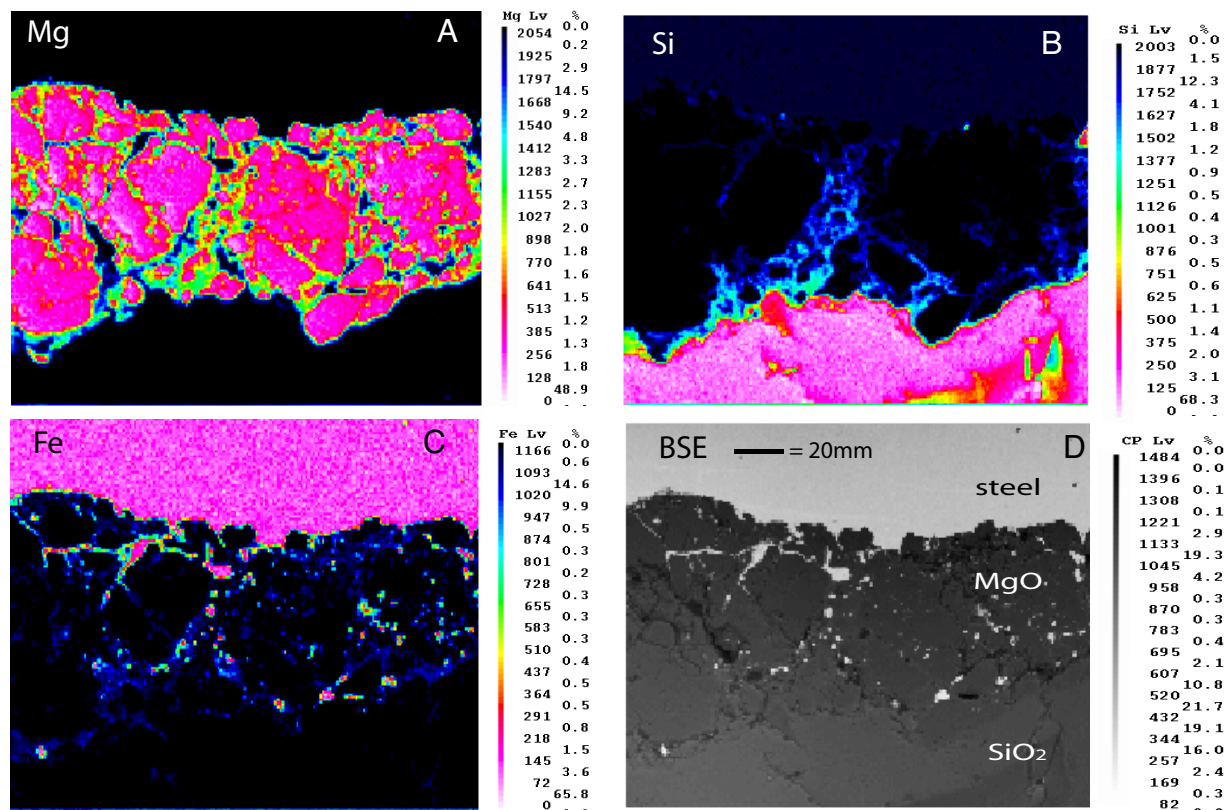
Fig. 1. Images and composition mapping of shocked sample S1210. (*A–C*) EMP wavelength-dispersive X-ray mapping of magnesium (*A*), silicon (*B*), and iron (*C*) concentration in section of shocked sample. (*D*) EMP backscattered electron (BSE) image of sample at 15-keV accelerating voltage. Color scales are labeled by count rates at each pixel (in counts/s per nA) and by histogram percentages of pixels in each intensity bin. In the BSE image, melted areas are clearly indicated by the fine scale dispersion of metal melt droplets (bright spots). In element concentration mappings, Fe-rich stainless-steel sample chamber (*Top*) and regions of sample originally consisting of porous MgO (*Middle*) and fused silica (*Bottom*) are clearly visible.

microscopy at beamline U2A, National Synchrotron Light Source; and electron backscatter diffraction (EBSD) analysis.

Analysis

Optical microscopy and EMP X-ray mapping of the sectioned and polished sample revealed a glassy magnesium silicate zone at the contact of the two sample materials (Fig. 1), which we presume quenched from a melt that digested to some extent both the MgO and SiO_2 starting materials. Within the silicate glass region we found abundant forsterite. The EMP mapping shows that quenched melt veins protrude from the silica–periclase boundary into bulk periclase and are indicated by their mixed composition. In some parts of the reaction boundary and the veins, melted metal from the chamber wall was injected (Fig. 1), forming veneers and arrays of very fine metallic droplets similar to observations from heavily shocked meteorites (14). The quenched glass has a composition approximating $(Mg_{0.95},Fe_{0.05})SiO_3$. The iron content of the silicate probably results from chemical interaction of immersed iron droplets and silicate melt, apparently based on a Fe–Si redox process. The metal droplets originate from the inner wall of the steel chamber but their composition has changed because of interaction with the molten silicate. In particular, the metal droplets contain between 1 and 2 atomic percent Si.

X-ray diffraction mapping (spatial resolution of several μm; see *Methods*) of the quenched silicate melt veins resulted in many patterns where 12–20 reflections were observed that match the unit cell of Mg_2SiO_4-wadsleyite. On this length scale wadsleyite is generally associated with olivine. Overlap of the powder diffraction patterns of both phases is substantial. Thus, we decided to reanalyze the sample by using EBSD (spatial resolution of 0.3 μm) and unambiguously confirmed the presence of multiple grains of wadsleyite mostly occurring in the vicinity of metal grains. Fig. 2 shows an indexed EBSD pattern. A unit cell of dimensions $5.70 \times 11.44 \times 8.26$ Å^3 has been fitted with mean angular deviation (MAD) of 0.659° (which is close to the resolution limit of 0.5°). In other cases, MAD varied between 0.5° and 0.8°. The observed cell closely matches reported cell parameters of wadsleyite (28). We speculate that shock temperature in the molten metal phase was lower than in the silicate melt formed from low-density silica glass and porous MgO. Proximity to metal droplets may have provided a locally high cooling rate such that preservation of this high-pressure polymorph occurred, whereas wadsleyite grains in the bulk of the silicate melt probably converted to forsterite. IR microscopy (spatial resolution, $10 \times 10 \ \mu m^2$) also confirmed the presence of a substantial amount of wadsleyite in our run product (Fig. 3).

Previous arguments for long shock durations in meteorites have not been restricted to simple occurrence of high-pressure phases but also considerations of their grain size, texture, and chemical diffusion profiles (15, 22–25). We therefore attempted to constrain the growth rate of the wadsleyite crystals in our experiment by using EBSD mapping (Fig. 2*B*). Such maps, where the crystal orientation is also known at each point, constrain the grain size of individual crystallites of wadsleyite to 1–3 μm and provide information about the matrix. In all cases wadsleyite was embedded in a glassy matrix that probably was quenched melt (Fig. 2*B*).

Mg_2SiO_4 wadsleyite forms at temperatures >2,000 K above 16 GPa (29). This pressure was reached after the second reverberation

Fig. 3. Reflectance IR spectrum of wadsleyite-bearing region compared with spectrum of forsterite collected from different regions of sample. Spatial resolution was $8 \times 10 \ \mu m^2$.

Fig. 2. Identification, grain size, and paragenesis of wadsleyite. (*A*) Indexed EBSD pattern with major bands and Miller indices of zone axes defining orientation. For clarity only bands with intensity (arbitrary units) >15 are labeled, but lowering the cutoff intensity shows that remaining bands are also wadsleyite reflections plus a few stray bands. The latter are a result of small crystallite dimensions. (*B*) Color-coded EBSD phase map of a region containing wadsleyite.

in our experiment, which implies that the growth of wadsleyite occurred over a duration of at most 500 ns if growth was constrained to the time interval between the second reverberation and the onset of release. In this case the corresponding average growth rate was 6 m/s. The volume self-diffusion coefficients of Si and O in molten midocean ridge basalt, komatiite, and peridotite at 2,300 K and 15–20 GPa can be estimated to be between 10^{-8} and 10^{-9} m²·s (30), implying diffusion-controlled growth rates of 10^{-3} to 10^{-4} m·s, which is 4–5 orders of magnitude slower than observed in our experiment. Thus, growth of wadsleyite in this experiment was not controlled by diffusion.

Discussion

It may be argued that sufficiently high pressure required to stabilize wadsleyite was not achieved over the entire 500 ns between the onset of the second reverberation and the inter-

ference of the rarefaction wave with the shock wave. Possibly the pressure and temperature range of thermodynamic stability of wadsleyite occurred only after the third reverberation, thus reducing growth times to ≈350 ns, which then implies even faster growth rates. Because no other high-pressure phase has been clearly identified in our experiment, it is also possible that the observed wadsleyite crystallized from shock-induced melt or transformation of higher-pressure polymorphs such as ringwoodite upon release from the shock state as the pressures decreased down to the 14- to 16-GPa range (29). In this range of pressure, temperature may have been too low to induce complete back-transformation, while any record of higher-pressure polymorphs may have been lost. In this case, the growth of wadsleyite occurred in much less than 500 ns. In all cases the entire period during which dynamic pressure remained >14 GPa was definitely too short to reconcile the average growth rate with a diffusion-controlled growth mechanism.

The observation of shock-induced formation of wadsleyite from a rapid nondiffusive growth process has several important implications bearing on our understanding of shock processes in meteorite parent bodies and for phase transformations under dynamic compression.

(*i*) The current consensus in planetary science that the occurrence of high-pressure silicate polymorphs in heavily shocked meteorites result from crystallization from shock-induced melts that remain at high pressure for long durations (seconds to minutes) as a result of large (≈1 to 100 km in diameter) planetesimal impacts is brought into question by the present results. Contrary to previous models, we produce shock-induced melt and subsequently crystallize a high-pressure polymorph, in this case wadsleyite, on a sub-μs time scale.

Arguments based on trace-element or major-element diffusion profiles (23) have been used to constrain the duration of elevated temperatures, but it remains to be seen whether chemically zoned growth from nondiffusive processes such as in our experiment or multiple shock events can mimic diffusion profiles. A recent study of the highly shocked Peace River chondrite supports this possibility by providing evidence that chemical zoning in a wadsleyite–ringwoodite aggregate resulted from fractional crystallization from a melt (31). Further, a suitable combination of postshock temperature and conductive cooling of shock-induced molten silicate veins could provide a preservation path that does not require long high-pressure duration.

(*ii*) The formation of μm-size crystals of the high-pressure-phase wadsleyite from a shock-induced melt on a sub-μs time scale appears to require a nondiffusive, shock-specific, and ultrafast growth mechanism. Such extremely efficient atomic-

scale mixing and reaction processes presumably also occurred in ancient very large-scale terrestrial impact events that produced extraordinarily homogeneous, 10^2 km in diameter, igneous-appearing melt sheets within structures such as Manicouagan and Sudbury.

Turbulent mass transport that scales with the particle velocity ($\approx 10^0$ to 10^1 km/s) in a shock-generated melt may provide a plausible basis for the inferred high growth rates.

(*iii*) Formation and width of ringwoodite lamellae in olivine (21, 22, 24) far from melt veins and pockets has been used as a constraint on shock duration in meteorites based on solid–solid transformation rates from static compression experiments. However, it is questionable whether growth under low-strain rate conditions in static experiments can directly be compared with growth under the high-strain rate conditions of shock metamorphosis. Our present results allow for cross-checking the shock duration derived from the width of ringwoodite lamellae by comparison with the size of wadsleyite grains in melt veins in the same meteorites.

(*iv*) Finally, this work may open paths for new methods of shock synthesis (and recovery) of other high-pressure phases via growth from the molten state. Many high-pressure phases have desirable properties, such as high hardness, but static devices generating pressures in excess of 5 GPa do not allow for producing economically relevant amounts. Shock synthesis, however, can be scaled up to large volumes.

Conclusions

We report the successful recovery of a high-pressure silicate polymorph, wadsleyite, from a shock experiment. In contrast to previous experimental studies, we generated shock temperatures high enough to allow for formation of a substantial amount of melt upon shock loading. Further, we used a combination of microscale diffraction and spectroscopic probes that allow for mapping rather large sample areas rather than being constrained (as in previous shock recovery studies) to extraction of a very small amount of sample for transmission electron microscopy analysis. Wadsleyite forms and grows from the shock-induced silicate melt to μm-length crystals on a sub-μs time scale, implying an ultrafast, nondiffusive growth mechanism that appears to be shock-specific. Our result implies that the occurrence and grain size of high-pressure phases in shocked meteorites alone does not require long shock durations and so does not require interactions between km-scale objects. Constraints on shock duration and hence on planetesimal sizes in the early solar system must take into account the actual rapid growth rates of crystallites forming in shock melts. For illustration: the size of a wadsleyite–ringwoodite aggregate grain grown from a shock-induced melt in the Peace River meteorite averages ≈ 60 μm in diameter (31), which is 20–100 times larger than the size of wadsleyite grains in our sample and therefore suggests growth within 10–100 μs in case of growth during the entire high-pressure shock interval. Assuming, for simplicity, that the Peace River event resulted from collision of two equally sized objects

at an impact velocity in the range of several km/s implies an object diameter of the order of <1 m. This diameter is surprisingly small, because meteorites are believed to be samples of much larger proto-planetary parent bodies. The parent bodies suffered energetic primordial collisions, and the present meteorites achieved this size as break-up fragments much earlier than encounter with the Earth.

Based on the present results we suggest that the interpretation of the high-grade shock-metamorphic record in meteorites needs a re-evaluation.

Methods

Micro X-ray diffraction was conducted in a backscattering geometry at the High Pressure Collaborative Access Team beamline IDB at Advanced Photon Source (APS) and at the dedicated microdiffraction beamline 7.3.3 at the Advanced Light Source (ALS) (32). A monochromatic beam of X-rays was focused to 5×5 μm^2 (APS) or 0.7×0.8 μm^2 (ALS) but penetration of the beam into the sample reduced lateral spatial resolution to ≈ 30 μm (APS) and ≈ 3 μm (ALS). Bragg diffraction was collected at fixed angular sample and detector positions with area detectors. At ALS beamline 7.3.3 a CCD detector mounted on the 2ϑ arm of a 6-circle goniometer was moved to position for collecting diffraction data in 45° backscattering geometry. Sample analysis at 16-IDB, APS, required modifications of the set-up: To achieve diffraction in reflection geometry over a range of 7° to 45° in 2ϑ we placed a MAR345 image plate detector at 450-mm distance from the sample such that the primary beam intersected the detector plane far off-center. An optical microscope was used for correlating sample position and primary beam. The primary beam was located by visible fluorescence of the MgO sample. The collected diffraction patterns were corrected for geometric distortion and integrated along the azimuthal angle in the detector plane by using the XMAS (31) software package.

IR microscopy was conducted in reflection geometry at beamline U2A, National Synchrotron Light Source using a 20× magnifying Schwartzschild objective and apertures resulting in a spatial resolution of 10 μm. EBSD analyses at a submicrometer scale were performed by using an HKL EBSD system on a Zeiss 1550VP field emission scanning electron microscope, operated at 20 kV and 8 nA in a focused beam with a 70° tilted stage. The EBSD system was calibrated by using a single-crystal silicon standard. Mean angular deviations for fits of wadsleyite unit cells ranged between 0.54° and <1.0°.

1. Tomioka N, Fujino K (2000) Shock-induced transition of NaAlSi3O8 feldspar into a hollandite structure in a L6 chondrite. *Geophys Res Lett* 27:3997–4000.
2. Gillet P, Chen M, Dubrovinsky L, El Goresy A (2000) Natural NaAlSi3O8-hollandite in the shocked Sixiangkou meteorite. *Science* 287:1633–1636.
3. Sharp TG, El Goresy A, Wopenka B, Chen M (1999) A post-stishovite SiO2 polymorph in the meteorite Shergotty: Implications for impact events. *Science* 284:1511–1513.
4. El Goresy A, Dubrovinsky L, Sharp TG, Saxena SK, Chen M (2000) A monoclinic post-stishovite polymorph of silica in the Shergotty meteorite. *Science* 288:1632–1634.
5. Dera P, Prewitt CT, Boctor NZ, Hemley RJ (2002) Characterization of a high-pressure phase of silica from the Martian meteorite Shergotty. *Am Min* 87:1018–1023.
6. Putnis A, Price GD (1979) High-pressure (Mg,Fe)2SiO4 phases in the Tenham chondritic meteorite. *Nature* 280:217–218.
7. Binns RA, Davis RJ, Reed SJB (1969) Ringwoodite natural (Mg,Fe)2SiO4 spinel in Tenham meteorite. *Nature* 221:943–944.
8. Smith JV, Mason B (1970) Pyroxene-garnet transformation in Coorara meteorite. *Science* 168:832–833.
9. Tomioka N, Kimura M (2003) The breakdown of diopside to Ca-rich majorite and glass in a shocked H chondrite. *Earth Planet Sci Lett* 208:271–278.
10. Tomioka N, Fujino K (1999) Akimotoite, (Mg,Fe)SiO₃, a new silicate mineral of the ilmenite group in the Tenham chondrite. *Am Min* 84:267–271.
11. Tomioka N, Fujino K (1997) Natural (Mg,Fe)SiO₃-ilmenite and -perovskite in the Tenham meteorite. *Science* 277:1084–1086.
12. Sharp TG, Lingemann CM, Dupas C, Stöffler D (1997) Natural occurrence of MgSiO₃-ilmenite and evidence for MgSiO₃-perovskite in a shocked L chondrite. *Science* 277:352–355.
13. Stöffler D (1997) Geoscience–Minerals in the deep earth: A message from the asteroid belt. *Science* 278:1576–1577.
14. Stöffler D, Keil K, Scott ERD (1991) Shock metamorphism of ordinary chondrites. *Geochim Cosmochim Acta* 55:3845–3867.

Tschauner et al.

15. Chen M, Sharp TG, El Goresy A, Wopenka B, Xie XD (1996) The majorite-pyrope plus magnesiowüstite assemblage: Constraints on the history of shock veins in chondrites. *Science* 271:1570–1573.

16. Xie ZD, Sharp TG, De Carli PS (2006) Estimating shock pressures based on high-pressure minerals in shock-induced melt veins of L chondrites. *Meteorit Planet Sci* 41:1883–1896.

17. DeCarli PS, Milton DJ (1965) Stishovite synthesis by shock wave. *Science* 147:144–145.

18. Kleeman JD, Ahrens TJ (1973) Shock-induced transition of quartz to stishovite. *J Geophys Res* 78:5954–5960.

19. Tschauner O, Luo S-N, Asimow PD, Ahrens TJ (2006) Recovery of stishovite-structure at ambient conditions out of shock-generated amorphous silica. *Am Min* 91:1857–1862.

20. Langenhorst F, Poirier JP, Deutsch A, Hornemann U (2002) Experimental approach to generate shock veins in single crystal olivine by shear melting. *Meteorit Planet Sci* 37:1541–1553.

21. Ohtani E, Kimura Y, Kimura M, Kubo T, Takata T (2004) Formation of high-pressure minerals in shocked L6 chondrite Yamato 791384: Constraints on shock conditions and parent body size. *Earth Planet Sci Lett* 227:505–515.

22. Xie ZD, Sharp TG (2007) Host rock solid-state transformation in a shock-induced melt vein of Tenham L6 chondrite. *Earth Planet Sci Lett* 254:433–445.

23. Beck P, Gillet P, El Goresy A, Mostefaoui S (2005) Time scales of shock processes in chondritic and Martian meteorites. *Nature* 435:1071–1074.

24. Chen M, Li H, El Goresy A, Liu J, Xie XD (2006) Fracture-related intracrystalline transformation of olivine to ringwoodite in the shocked Sixiangkou meteorite. *Meteorit Planet Sci* 41:731–737.

25. Price GD, Putnis A, Agrell SO (1979) Electron petrography of shock-produced veins in the Tenham chondrite. *Contrib Mineral Petrol* 71:211–218.

26. Kimura M, Chen M, Yoshida Y, El Goresy A, Ohtani E (2004) Back-transformation of high-pressure phases in a shock melt vein of an H-chondrite during atmospheric passage: Implications for the survival of high-pressure phases after decompression. *Earth Planet Sci Lett* 217:141–150.

27. Luo S-N, Swift DC, Mulford RN, Drummond ND, Ackland GJ (2004) Performance of an ab initio equation of state for magnesium oxide. *J Phys Condens Matt* 16:5435–5442.

28. Horiuchi HE, Sawamoto H (1981) β-Mg$_2$SiO$_4$: Single-crystal X-ray diffraction study. *Am Min* 66:568–575.

29. Morishima H, et al. (1994) The phase-boundary between α-Mg$_2$SiO$_4$ and β-Mg$_2$SiO$_4$ determined by in situ X-ray observation. *Science* 265:1202–1203.

30. Guillot B, Sator N (2007) A computer simulation study of natural silicate melts. Part II: High-pressure properties. *Geochim Cosmochim Acta* 71:4538–4556.

31. Miyahara M, et al. (2008) Evidence for fractional crystallization of wadsleyite and ringwoodite from olivine melts in chondrules entrained in shock-melt veins. *Proc Natl Acad Sci USA* 105:8542–8547.

32. Tamura N, et al. (2003) Scanning X-ray microdiffraction with submicrometer white beam for strain/stress and orientation mapping in thin films. *J Synchrotron Radiat* 10:137–143.

GEOPHYSICS